Rare Metal Materials and Engineering
Volume 49, Issue 8, August 2020
Available online at www.rmme.ac.cn

Science Press

Cite this article as: Rare Metal Materials and Engineering, 2020, 49(8): 2591-2598.

ARTICLE

Constitutive Behavior and Processing Map of As-cast Mg-8Y-6Gd-1Nd-0.17Zn Magnesium Alloy Compressed at Elevated Temperatures

Liu Chongliang[1], Quan Gaofeng[1], Zhou Mingyang[2], Guo Yangyang[1], Fan Ling-ling[1]

[1] *Key Laboratory of Advanced Technologies of Materials, Ministry of Education, Southwest Jiaotong University, Chengdu 610031, China;*
[2] *Science and Technology on Reactor System Design Technology Laboratory, Nuclear Power Institute of China, Chengdu 610213, China*

Abstract: The constitutive behavior and hot workability of as-cast Mg-8Y-6Gd-1Nd-0.17Zn magnesium alloy during the hot compression were investigated at elevated temperature (350~450 °C) and different strain rates (0.0001~0.1 s^{-1}) under the ultimate compression ratio of 50%. The relationship among these deformation parameters of Mg-8Y-6Gd-1Nd-0.17Zn alloy was characterized by a sine hyperbolic equation. The experimental results show that both temperature and strain rate have important effects on the flow stress behavior of Mg-8Y-6Gd-1Nd-0.17Zn magnesium alloy, and the flow stress increases at lower temperature and higher strain rates. Typical dynamic recrystallization character is found in the true stress-strain curves when samples are compressed at the temperature above 400 °C. The activation energy (Q) and stress exponent (n) during deformation are 359.258 kJ/mol and 5.24, respectively. The average error (ARE) between experimental and calculated values is 3.37%. Then, the processing maps are also established and analyzed based on dynamic material model. Considering the processing maps and microstructure observation, the optimum hot-working parameters of the alloy are determined to be temperatures of 400~450 °C and strain rates of 0.0001~0.001 s^{-1}.

Key words: Mg-Gd-Y-Nd-Zn magnesium alloy; hot compression; microstructure evolution; constitutive equation; processing map

Magnesium alloys, as “the 21st century green engineering metal materials”, have been employed in the fields of 3C electronic products, high-speed railways, and aerospace, with their excellent combination of lightweight and good performance[1-3]. Unfortunately, the poor plasticity and formability of magnesium alloy at room temperature restrict their application owning to their hexagonal close-packed crystal (hcp) structure with a limited number of easily activated slip systems. Therefore, the wrought magnesium alloys used in industrial applications are prior to complete under hot conditions to improve their forming properties[4,5]. So it is of great significance to investigate the plastic deformation behavior of magnesium alloy at high temperature and master the high temperature deformation mechanism of magnesium alloy to promote the application of magnesium alloys in various fields.

Nowadays, much attention was focused on the study of hot deformation behavior of Mg-RE alloys compared with Mg-Al or Mg-Zn alloys, since the addition of rare earth elements in magnesium alloy can significantly improve its room and high temperature performance and creep resistance[6-8]. Jiang[9] et al studied the strain-hardening and warm deformation behavior of extruded Mg-Sn-Y alloy sheet. They used the Kocks-Mecking type plots to show different stages of strain hardening and found that the decrease of strain hardening ability of the alloy after yielding is attributed to the reduction of dislocation density with increasing the testing temperature. Lu[10] et al investigated the hot compression deformation

Received date: August 11, 2019
Foundation item: Key Development Project of Sichuan Province (2017GZ0399); 2017 Doctoral Innovation Fund Program of Southwest Jiaotong University (D-CX201733)
Corresponding author: Quan Gaofeng, Ph. D., Professor, Key Laboratory of Advanced Technologies of Materials, Ministry of Education, School of Materials Science and Engineering, Southwest Jiaotong University, Chengdu 610031, P. R. China, Tel: 0086-28-87634673, E-mail: quangf@swjtu.edu.cn

behavior of Mg-Gd-Y-Zn-Zr alloy, and the processing map indicates that this alloy exhibits a better hot workability at 0.1 s^{-1}/480 °C. Lu[11] et al researched the tensile and compressive deformation behavior of the peak aged cast Mg-11Y-5Gd-2Zn-0.5Zr magnesium alloy under the conditions of 25~400 °C and 10^{-4}~10^{-2} s^{-1}, and established the high temperature deformation constitutive equation and the main high temperature deformation mechanism of the alloy was also inferred based on the deformation activation energy.

Therefore, the aim of this presented work is to investigate the high temperature compression behavior and hot workability of Mg-8Y-6Gd-1Nd-0.17Zn RE magnesium alloy at elevated temperature and strain rates by developing a constitutive equation and processing map. A sine hyperbolic equation was developed to characterize the relationship of deformation parameters. The optimum hot-working condition of Mg-8Y-6Gd-1Nd-0.17Zn magnesium alloys was identified from the microstructure observation and processing map, which provides a research basis for the thermoplastic deformation and subsequent thermoforming of the alloy.

1 Materials and Methods

The experimental material employed in this research was a high-strength heat-resistant RE magnesium alloy. The actual chemical composition was measured by inductively coupled plasma-atomic emission spectrometer (ICP-AES), as shown in Table 1.

Cylindrical testing samples were machined into 10 mm in diameter and 15 mm in height using an electro-discharge machine. The isothermal compression tests were conducted using a MTS-CMT5105 universal testing machine equipped with an electrical furnace at the temperature ranging from 350 °C to 450 °C with strain rates ranging from 0.0001 s^{-1} to 0.1 s^{-1}. Prior to compression testing, the samples were held at a specified temperature for 10 min. In order to decrease the influence of friction between the sample and the indenter on the experiment, graphite sheets were coated on the upper and lower surfaces of the sample as lubricant during compression. In this study, at least three tests were conducted for each experimental condition.

The maximum comparative gauge reduction of all the specimens was 50%. After the samples were compressed, the specimens were water quenched immediately at 25 °C to retain the character of deformed microstructure. Subsequently, the specimens were sectioned for metallographic analysis. A Zeiss microscope (Zeiss Lab.A1) and scanning electron microscope (SEM) with energy dispersive spectrometer (EDS) were used to observe the microstructure.

Table 1 Chemical composition of Mg-8Y-6Gd-1Nd-0.17Zn magnesium alloy (wt%)

Y	Gd	Nd	Zn	Mg
7.45	5.93	0.97	0.17	Bal.

2 Results and Discussion

2.1 Initial microstructure

Fig.1 shows the typical microstructure of as-cast Mg-8Y-6Gd-1Nd-0.17Zn alloy. The average grain size is about 71.7±2.5 μm. It can be seen that the microstructure consists of primarily α matrix and network eutectic β phase at the grain boundaries which is shown in Fig.1a. The grain boundary is clear but coarse and the grains are irregular. The discontinuous network consists mainly of a skeletal eutectic phase (D) at the grain boundary, a gray bulk phase (C), and a free rare earth-rich white phase (B) near the grain boundary, which are shown in Fig.1b. EDS analysis of the second phase of the alloy shows that RE elements Y and Gd are enriched at point B, which can be inferred to be Mg_5Gd phase by the atomic percentage. The atomic percentage of Mg-8.67Y-6.01Gd-1.03Nd-0.3Zn (at%) indicates that the phase may be Mg_5(Y, Gd) at point D. The energy spectrum analysis results of the magnesium alloy are shown in Table 2.

2.2 True stress-strain curves

Fig.2 shows the true stress-strain curves of Mg-8Y-6Gd-1Nd-0.17Zn magnesium alloy deformed under different

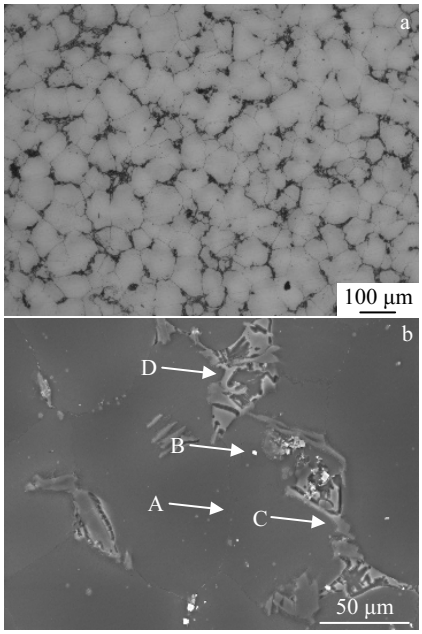

Fig.1 OM (a) and SEM (b) images of as-cast Mg-8Y-6Gd-1Nd-0.17Zn magnesium alloy

Table 2 EDS analysis results of marked points for as-cast Mg-8Y-6Gd-1Nd-0.17Zn magnesium alloy in Fig.1b (at%)

Point	Mg	Gd	Nd	Y	Zn	Possible phase
A	96.17	1.03	0.15	2.65	-	-
B	30.68	6.66	0.42	62.24	-	Mg_5Gd
C	89.6	1.56	0.20	4.19	0.61	-
D	83.92	6.01	1.03	8.67	0.30	Mg_5(Y, Gd)

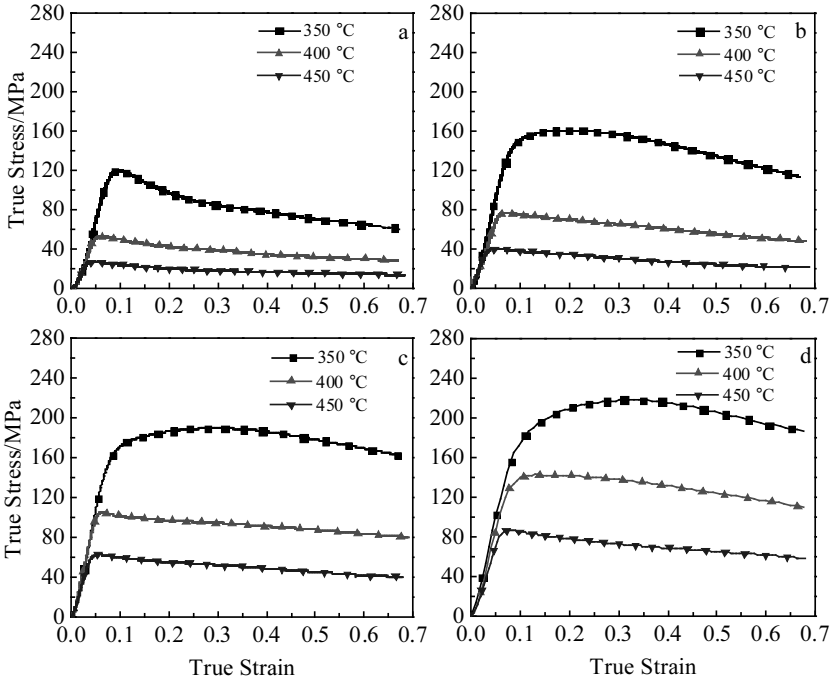

Fig.2 True stress-strain curves of Mg-8Y-6Gd-1Nd-0.17Zn alloy under different conditions: (a) $\dot{\varepsilon}$=0.0001 s^{-1}, (b) $\dot{\varepsilon}$=0.001 s^{-1}, (c) $\dot{\varepsilon}$=0.01 s^{-1}, and (d) $\dot{\varepsilon}$=0.1 s^{-1}

conditions. It can be found that both temperatures and strain rates exert significantly effects on the flow stress behavior under all the tested conditions. In general, the flow stress decreases with decreasing the strain rate and increasing the temperature. This absolutely follows the trend behavior of metallic alloy in hot working[12].

It can be seen that obvious difference exists in the true stress-strain curves, as shown in Fig.2. The flow stress of Mg-8Y-6Gd-1Nd-0.17Zn alloy increases rapidly with the increase of strain before reaching the peak stress during plastic deformation at the initial deformation stage. The curve shows obvious work hardening characteristics during plastic deformation at 350 °C, while at higher temperatures, the work hardening ability decreases gradually. When deformation occurs at temperature above 400 °C, the flow stress decreases slowly after reaching the peak stress and is gradually in a steady stage, which is in line with the typical dynamic recrystallization (DRX) curve composed of following three stages: work-hardening, dynamic softening, and steady flow stage[13], illustrating that dynamic recrystallization plays a role in decreasing stress. To some extent, the softening effect caused by the dynamic recrystallization (DRX) and dynamic recovery (DRV) is insufficient when the temperature is lower than 400 °C, and the steady-state flow stage is almost nonexistent.

Fig.3a and 3b demonstrate the effect of temperature and strain rate on UTS of the alloy, respectively. The peak stress decreases with increasing the temperature at a constant strain rate (the peak stress decreases from 159.98 MPa to 40.01 MPa when temperature increases from 350 °C to 450 °C at a strain rate of 0.001 s^{-1}). This is because as the deformation

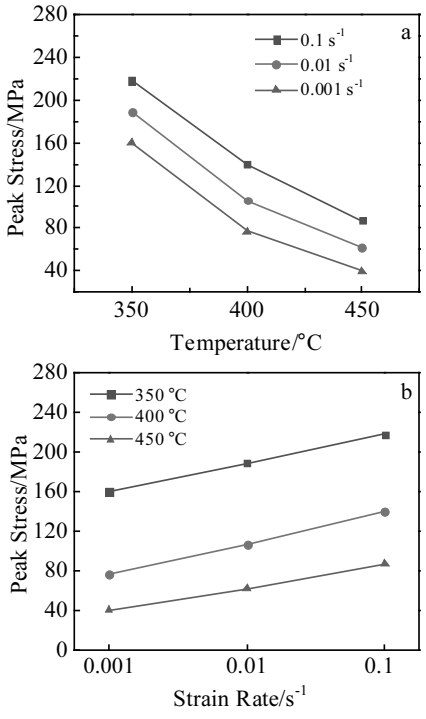

Fig.3 Effects of temperature (a) and strain rate (b) on the peak stress of as-cast Mg-8Y-6Gd-1Nd-0.17Zn magnesium alloy under different conditions

temperature increases, the diffusion of atoms is strengthened, and the slip, climb, and slip of the dislocations are easier than those at lower temperature, so the softening effect in the deformation process is more prominent. Similarly, the peak value decreases with decreasing the strain rate at a given temperature (the peak stress decreases from 140.46 MPa to 54.29 MPa when the strain rate decreases from 0.1 s^{-1} to 0.0001 s^{-1} at temperature of 400 °C), because higher dislo- cation density appears in the crystal at higher strain rates, which hinders the movement of dislocations. At the same time, lower strain rates and higher temperatures provide a longer time for nucleation and growth of dynamic recrystallized grains and dislocation annihilation that reduce the flow stress level. Table 3 shows the value of peak stress under different deformation conditions.

2.3 Constitutive equation

The high temperature deformation constitutive equation of the material reflects the relationship between the flow stress and the thermodynamic parameters, and is also the basis for the computer simulation of the thermal processing[14,15]. The relationship of the deformation temperature, peak stress and strain rate can be described by the following sine hyperbolic equation for Mg alloys[16-18]:

$$\dot{\varepsilon} = A[\sinh(\alpha\sigma)]^n \exp(-Q/RT) \quad (1)$$

where A, α are material constants, σ is the flow stress, $\dot{\varepsilon}$ is the strain rate, T is absolute temperature, n is exponent of stress, Q is activation energy of deformation, R is the ideal universal constant (R=8.314 J·mol^{-1}·k^{-1}).

According to different flow stresses[19], the constitutive equation can be expressed as the following equations:

$$\dot{\varepsilon} = A_1 Q^n \exp(-Q/RT) \ (\alpha\sigma < 0.8) \quad (2)$$

$$\dot{\varepsilon} = A_2 \exp(\beta\sigma) \exp(-Q/RT) \ (\alpha\sigma > 1.2,\ \alpha=\beta/n) \quad (3)$$

Eq.(4) and Eq.(5) are derived by Eq.(2) and Eq.(3), respectively.

$$1/\beta = (\partial\sigma/\partial\ln\dot{\varepsilon})_T \quad (4)$$

$$1/n = (\partial\ln\sigma/\partial\ln\dot{\varepsilon})_T \quad (5)$$

In this work, the value of peak stress was used for the fitting. Fig.4 shows the results of the linear fitting of σ-ln$\dot{\varepsilon}$ and lnσ-ln$\dot{\varepsilon}$. The value of 1/β can be obtained by the average slope value of the lines under the condition of high stress, while the value of 1/n was obtained under the condition of low stress, so $\alpha=\beta/n$=0.0125 MPa^{-1}.

The exponent of stress n and the activation energy of hot deformation Q can be obtained from the following two formulas.

$$1/n = m = \{\partial[\ln\sinh(\alpha\sigma)]/\partial\ln\dot{\varepsilon}\}_T \quad (6)$$

Table 3 Peak stress of as-cast Mg-8Y-6Gd-1Nd-0.17Zn magnesium alloy compressed at elevated temperatures

Strain rates/s^{-1}	Values of peak stress/MPa		
	350 °C	400 °C	450 °C
1×10^{-1}	218.25	140.46	86.73
1×10^{-2}	189.00	106.13	61.98
1×10^{-3}	159.98	76.93	40.01

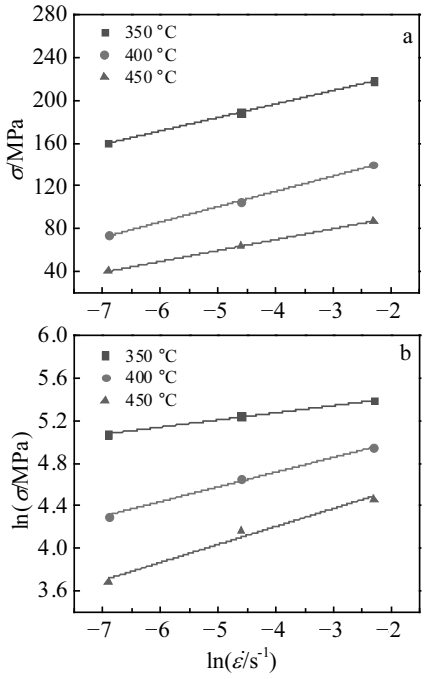

Fig.4 Relationship of σ-ln$\dot{\varepsilon}$ (a) and lnσ-ln$\dot{\varepsilon}$ (b) under different deformation conditions

$$Q = nR\{\partial[\ln\sinh(\alpha\sigma)]/\partial(1/T)\}_{\dot{\varepsilon}} \quad (7)$$

Fig.5 shows the results of the linear fitting of ln[sinh($\alpha\sigma$)]-ln$\dot{\varepsilon}$ and ln[sinh($\alpha\sigma$)]-T^{-1}. Similarly, n and Q can be calculated by Fig.5: n =5.24, Q=359.258 kJ/mol.

Finally, the constant A is obtained by Eq.(2); taking logarithm on both sides of Eq.(2), we can obtain:

$$\ln Z = \ln A + \ln\sinh(\alpha\sigma) \quad (8)$$

where ln$A$ was the y-intercept of Fig.6, and A is 2.82×10^{24} after calculation.

Therefore, the constitutive model of the Mg-8Y-6Gd-1Nd-0.17Zn alloy at temperatures from 350 °C to 450 °C and strain rates from 0.0001 s^{-1} to 0.1 s^{-1} can be described as following equation:

$$\dot{\varepsilon} = 2.82\times10^{24}[\sinh(0.0125\sigma)]^{5.24} \exp(-\frac{359258}{RT}) \quad (9)$$

Once any two value of $\dot{\varepsilon}$, σ and T are obtained, the third one can be acquired from Eq.(9). The average error (ARE) of experimental values and calculated values is given as:

$$\mathrm{ARE} = \frac{1}{N}\sum_i^N \left[\left|\frac{\sigma_{\mathrm{meas}} - \sigma_{\mathrm{pre}}}{\sigma_{\mathrm{meas}}}\right|\right]\times100\% \quad (10)$$

Table 4 shows the results of comparison between experimental and calculated values. ARE is 3.37% calculated by Eq.(10), which means that Eq.(9) can accurately describe the behavior of the as-cast Mg-8Y-6Gd-1Nd-0.17Zn magnesium alloy during hot working within a range of temperatures.

2.4 Microstructure evolution

Fig.7 shows the micrographs of the as-cast Mg-8Y-6Gd-

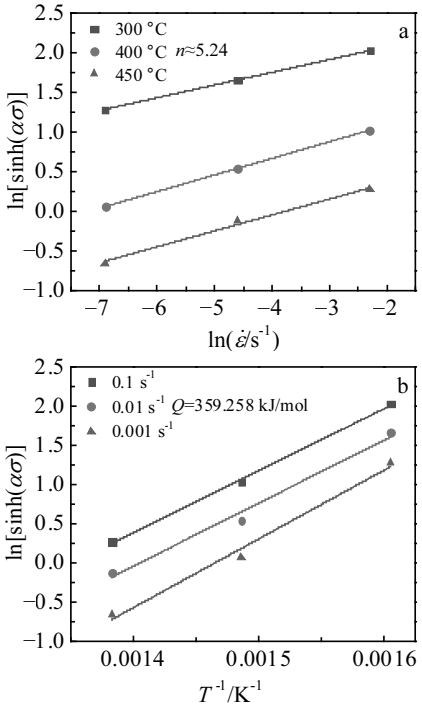

Fig.5 Relationship of $\ln[\sinh(\alpha\sigma)]$-$\ln\dot{\varepsilon}$, illustrating the determination of the stress exponent n (a); $\ln[\sinh(\alpha\sigma)]$-T^{-1}, illustrating the determination of the activation energy Q (b)

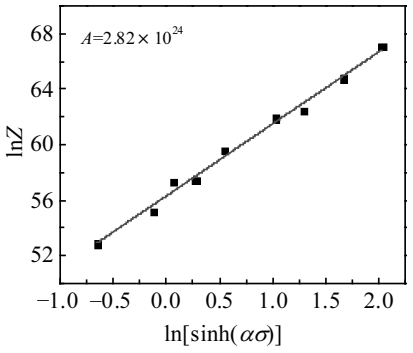

Fig.6 Linear relationships of ln$Z$-ln[sinh($\alpha\sigma$)]

Table 4 Experimental data and calculation value of peak stress of as-cast Mg-8Y-6Gd-1Nd-0.17Zn magnesium alloy

Temperature/ °C	Strain rate/s^{-1}	Experimental value/MPa	Predicted value/MPa	Error/%
350	0.1	218.25	220.05	0.82
	0.01	189.00	185.39	1.91
	0.001	159.98	151.35	5.39
400	0.1	140.46	143.30	2.02
	0.01	106.13	110.98	4.57
	0.001	76.93	81.87	6.42
450	0.1	86.73	83.80	3.38
	0.01	61.98	59.02	4.81
	0.001	40.01	39.89	0.27

1Nd-0.17Zn alloys compressed under different conditions. It can be found that almost all grains are elongated in the direction perpendicular to the compression axis at all deformation temperatures. The microstructures of samples compressed at 0.001 s^{-1} with different temperatures are shown in Fig.7a~7c. No recrystallized grains can be observed inside the original grains or along the grain boundaries at the deformation temperature of 350 °C. When the alloy is compressed at higher temperatures (400 and 450 °C), a great number of recrystallized grains appear in the interior of original grains.

Strain rates also has remarkable effects on the deformation microstructures[20]. Fig.7c~7e show the microstructures of alloys deformed at 450 °C with different strain rates. As shown, the recrystallized grains can be observed obviously inside the grains at this temperatures and higher strain rate can result in smaller grains. The stress-strain curve can reflect the change of microstructure of the alloy during deformation, and the flow softening seems more pronounced at a lower strain rate than at higher strain rate, which is evident from Fig.2, Fig.7c and Fig.7e. Also, the degree of dynamic recrystallization decreases as the strain rate increases. When the compression rate is fast, there is no enough time for dislocations to consume and dynamic recrystallization grains to grow with the increase of accumulated energy.

2.5 Processing map

The processing map which is based on the theory of dynamic materials models (DMM) is an important model for optimizing the hot processing parameters[21]. By meanings of the processing map, the plastic deformation under different conditions can be predicted, and the danger or instability deformation domains can also be avoided. According to the theory of dissipation[22], the instantaneous dissipation power P consists of two complementary parts: G and J content. In this model, G and J are correlated to the strain rate sensitivity as follows:

$$\left(\frac{\partial J}{\partial G}\right)_{\dot{\varepsilon},T}=\left[\frac{\partial(\ln\sigma)}{\partial(\ln\dot{\varepsilon})}\right]_{\dot{\varepsilon},T}=m \tag{11}$$

where m means the strain rate sensitivity. The content of G is related to the energy dissipation during plastic deformation, most of which are converted into heat. The content of J represents the energy dissipation during the transformation of microstructures, such as dynamic recrystallization and damage of the material.

For an ideal linear dissipating processing, m=1, and J reaches its maximum, $J_{max}=\sigma\dot{\varepsilon}/2$. The efficiency of power dissipation η occurring through microstructural changes during compression as a function of temperature and strain rate is given by follows:

$$\eta=\frac{J}{J_{max}}=\frac{2m}{m+1} \tag{12}$$

According to the principle of irreversible thermodynamic extremum, dimensionless parameter ξ is used to express the

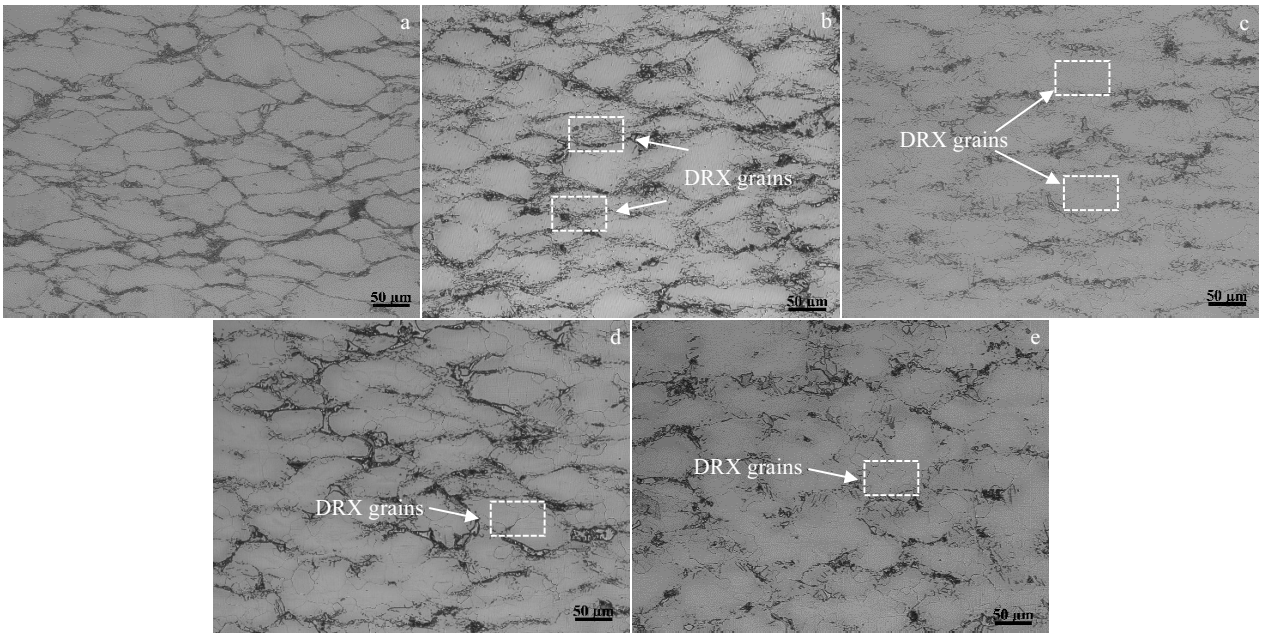

Fig.7 Microstructures of the as-cast Mg-8Y-6Gd-1Nd-0.17Zn-0.15Ni magnesium alloy after high temperature compression test: (a) 350 °C, 10^{-3} s^{-1}; (b) 400 °C, 10^{-3} s^{-1}; (c) 450 °C, 10^{-3} s^{-1}; (d) 450 °C, 10^{-2} s^{-1}; (e) 450 °C, 10^{-1} s^{-1}

criterion of continuous instability in deformation. The expression is follows:

$$\xi(\dot{\varepsilon}) = \frac{\partial \ln(\frac{m}{m+1})}{\partial \ln \dot{\varepsilon}} + m < 0 \quad (13)$$

The dependence of instability parameters $\xi(\dot{\varepsilon})$ on strain rates and temperatures can be expressed by the instability map.

The processing maps of the alloy obtained at different strains are shown in Fig.8. The shaded domain in the maps represents the instability processing region and figures represent sufficiency of power dissipation η. From the following processing maps, there are some differences between each map especially when the strain is higher than 0.5. It can be seen that the unstable area (domain B) decreases and is replaced by instability domain (the shaded domain) gradually with increasing the strain. That is to say, the instability domain increases with the strain, especially at the areas with higher strain rates. The safe zone (domain A) of maps is mainly concentrated in areas with lower strain rates (0.001 and 0.0001 s^{-1}) when the strain increases from 0.2 to 0.6. Here, the values of η represent the degree of dynamic recrystallization of the alloy during high temperature deformation. Generally speaking, the materials deformed in the condition with a higher efficiency of power dissipation show better workability[23]. But unstable flow may also occur when η is high. Therefore, the temperature and strain rate corresponding to the peak η in safe processing region should be the optimum parameters for hot working.

The processing map obtained at a strain of 0.5 from flow stress is shown in Fig.8c. This map exhibits four domains including one safe area, two instability areas and one unstable domain. The safe domain A has the highest peak efficiency of power dissipation at 0.3640, which occurs in temperature and strain rate ranges of 380~450 °C, 0.0001~0.001 s^{-1} and the 400~450 °C, 0.001~0.01 s^{-1}, respectively. The parameters of each domains of the processing map at strain of 0.5 are shown in Table 5. However, the instability domains is always accompanied with the characteristic of flow localization, cracks, kinking, adiabatic shear bands, etc[24]. Instability microstructures (400 °C and 0.1 s^{-1}, 450 °C and 0.1 s^{-1}) due to flow localization in the instability domain D are shown in Fig.9a and 9b. DRX is not observed in Fig.9a and micro voids which can be regard as the causes of the initial cracks are also observed along the grain boundaries in Fig.9a and 9b. As for another region C (350 °C and 0.001 s^{-1}), we can hardly find the DRX grains.

According to the research that DRX is a beneficial process in hot deformation and the deformation mechanisms in safe domains also correspond to the DRX and DRV[24,25]. As shown in Fig.7b~7d, dynamic recrystallization is also observed in safe domain A for the sample. The sample deformed in domain A exhibits completed DRX grains which can provide good intrinsic workability both by softening and reconstituting the microstructure. In this study, the contour lines for domain A are not dense, which provides a relatively

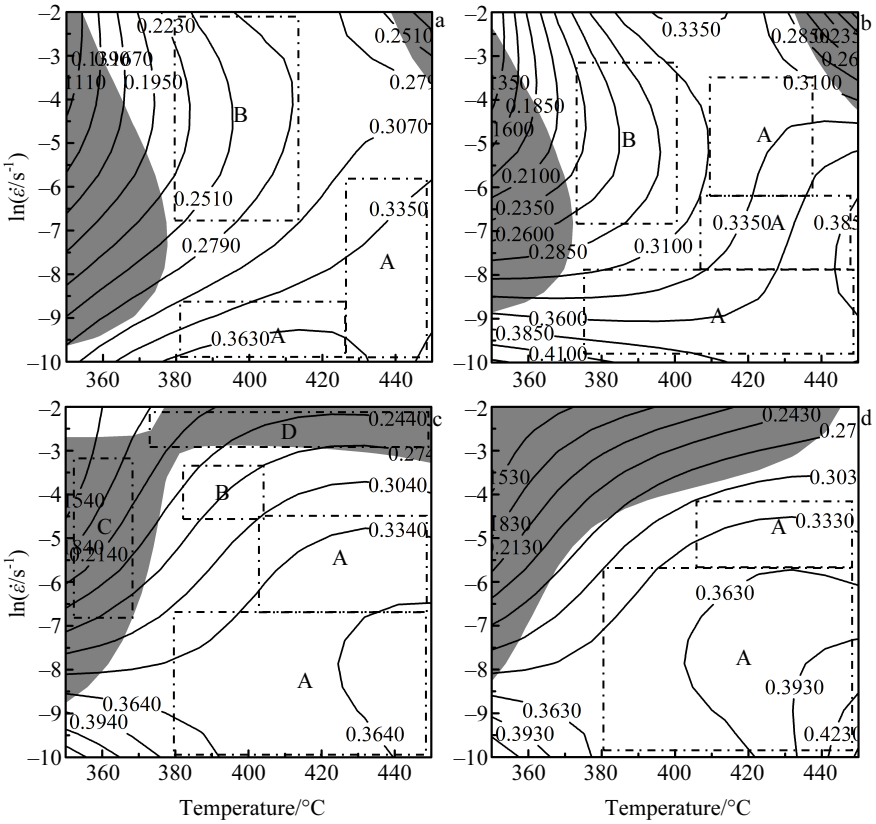

Fig.8 Processing maps of the Mg-8Y-6Gd-1Nd-0.17Zn alloy at different strains: (a) 0.2, (b) 0.4, (c) 0.5, and (d) 0.6

Table 5 Processing map parameters of Mg-8Y-6Gd-1Nd-0.17Zn alloy at strain of 0.5

Domain	Temperature/°C	Strain rate/s^{-1}	Peak sufficiency, η	ξ
A	380~450	0.0001~0.001	0.3640	>0
	400~450	0.001~0.01	0.3340	>0
B	380~400	0.01	0.2740	>0
C	350~360	0.001~0.01	0.3040	<0
D	380~450	0.1	0.2740	<0

large window for safe processing. Therefore, the processing map exhibits a deformation domain of complete DRX occurred, which is the optimum parameter for hot working such as hot extruding, hot rolling and hot forging of the alloy. The optimum hot-working condition for the specimen is determined to be a temperature range of 400 ~450 °C and a strain rate of 0.0001~0.001 s^{-1}.

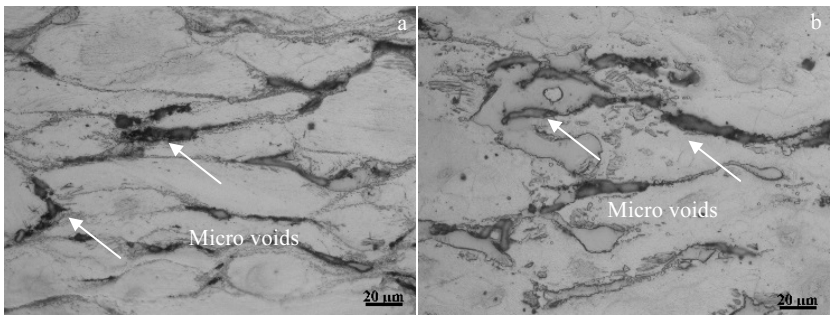

Fig.9 Microstructures of the alloys compressed at a strain rate of 0.1 s^{-1} at 400 °C (a) and 450 °C (b)

3 Conclusions

1) Temperature and strain rate have important effects on the flow stress behavior of Mg-8Y-6Gd-1Nd-0.17Zn magnesium alloy. The true stress-strain curves exhibit typical dynamic recrystallization character that the flow stress reaches a peak stress and then decreases slowly and approaches a stable state gradually at the temperature above 400 °C.

2) The flow stress of Mg-8Y-6Gd-1Nd-0.17Zn alloy can be symbolized by a hyperbolic-sine-type equation expressed as follows:

$$\dot{\varepsilon} = 2.82 \times 10^{24} [\sinh(0.0125\sigma)]^{5.24} \exp(-\frac{359258}{RT})$$

The stress exponent n and the activation energy of deformation Q are 5.24 and 359.258 kJ/mol, respectively.

3) The average error between experimental values and calculated values is 3.37%, which means that the equation can accurately predict the high temperature deformation flow stress of as-cast Mg-8Y-6Gd-1Nd-0.17Zn magnesium alloy.

4) According to the processing map and microstructure observation, the optimum hot-working conditions for as-cast Mg-8Y-6Gd-1Nd-0.17Zn alloy are determined to be a temperature range of 400~450 °C and a strain rate of 0.0001~0.001 s^{-1}.

References

1 Wu Z X, Curtin W A. *Nature*[J], 2015, 526(7571): 62

2 Luo, Alan A. *Journal of Magnesium and Alloys*[J], 2013, 1(1): 2

3 Ren L B, Quan G F, Boehlert C J *et al*. *Metallurgical and Materials Transactions A*[J], 2018, 49(8): 3692

4 Yin D D, Wang Q D, Boehlert C J *et al*. *Metallurgical and Materials Transactions A*[J], 2012, 43(9): 3338

5 Zheng L, Liu C M, Jin J *et al*. *Journal of Materials Engineering and Performance*[J], 2013, 22(1): 104

6 Ren L B, Quan G F, Zhou M Y *et al*. *Materials Science and Engineering A*[J], 2017, 690: 195

7 Zhao Z W, Teng X Y, Zhou G R *et al. Rare Metal Materials and Engineering*[J], 2014, 43(4): 791

8 Cui Chunxiang, Wu Renhao, Wang H W. *Rare Metal Materials and Engineering*[J], 1997(3): 53

9 Jiang J, Bi G L, Wang G Y *et al. Journal of Magnesium and Alloys*[J], 2014, 2(2): 116

10 Lu G, Xie Z P, Zhang Z M *et al*. *Applied Mechanics and Materials*[J], 2014, 680: 15

11 Lu J W, Yin D D, Ren L B *et al*. *Journal of Materials Science*[J], 2016, 51(23): 10 464

12 Wu H Y, Yang J C, Zhu F J *et al. Materials Science and Engineering A*[J], 2013, 574: 17

13 Lin Y C, Chen M S, Zhou J. *Mechanics Research Communications*[J], 2008, 35(3): 142

14 Zhou Mingyang, Su Xinxin, Ren Lingbao *et al. Rare Metal Materials and Engineering*[J], 2017, 46(8): 2149 (in Chinese)

15 Slooff F A, Zhou J, Duszczyk *et al. Scripta Materialia*[J], 2007, 57(8): 759

16 Mirzadeh, Hamed. *Mechanics of Materials*[J], 2014, 77: 80

17 Xia Xiangsheng, Chen Qiang, Zhang Kui *et al. Materials Science and Engineering A*[J], 2013, 587: 283

18 Kim W J, Kwak T Y. *Metals and Materials International*[J], 2017, 23(4): 660

19 Evangelista E, Spigarelli S. *Metallurgical and Materials Transactions A*[J], 2002, 33(2): 373

20 Li L, Murάnsky Ondrej, Flores-johnson E A *et al. Materials Science & Engineering A*[J], 2017, 684: 37

21 Sani S A, Ebrahimi G R, Vafaeenezhad H *et al. Journal of Magnesium and Alloys*[J], 2018, 6(2): 134

22 Prasad Y V R K. *Journal of Materials Engineering and Performance*[J], 2003, 12(6): 638

23 Yang Y B, Xie Z P, Zhang Z M *et al. Materials Science and Engineering A*[J], 2014, 615: 183

24 Qin Q F, Tan Y X, Zhang Z M *et al. Journal of Materials Engineering and Performance*[J], 2016, 25(1): 304

25 Zhou H, Wang Q D, Ye B *et al. Materials Science and Engineering A*[J], 2013, 576: 101

铸态 Mg-8Y-6Gd-1Nd-0.17Zn 稀土镁合金高温压缩本构行为及加工图

刘崇亮[1]，权高峰[1]，周明扬[2]，郭阳阳[1]，范玲玲[1]

(1. 西南交通大学 材料先进技术教育部重点实验室，四川 成都 610031)

(2. 中国核动力研究设计院 核反应堆系统设计技术重点实验室，四川 成都 610213)

摘　要：研究了铸态 Mg-8Y-6Gd-1Nd-0.17Zn 镁合金在应变量为 50%、温度 350~450 ℃、应变速率 0.0001~0.1 s^{-1} 条件下热压缩过程中的本构行为、组织演变和热加工性能。选用双曲正弦本构方程描述合金的流变行为以及变形参数间的关系。结果表明，温度和应变速率对 Mg-8Y-6Gd-1Nd-0.17Zn 镁合金的流变应力行为有重要影响，其流变应力随温度的降低和应变速率的增加而增大，并且在温度高于 400 ℃ 压缩时，合金的真应力应变曲线具有典型的动态再结晶特性。在本实验条件下，该合金变形期间的活化能（Q）和应力指数（n）分别为 359.258 kJ/mol 和 5.24，实验值与计算值之间的平均误差（ARE）为 3.37%。最后基于动态材料模型加工理论，结合热加工图和压缩过程中的组织演变，确定了该合金的最佳热加工参数为：加热温度 400~450 ℃，应变速率为 0.0001~0.001 s^{-1}。

关键词：Mg-Gd-Y-Nd-Zn 镁合金；热压缩；微观结构演变；本构方程；热加工图

作者简介：刘崇亮，男，1995 年生，硕士，西南交通大学材料科学与工程学院，四川 成都 610031，电话：028-87634673，E-mail: 815905485@qq.com